J BONE ONCOL 47 (2024) 100617

Contents lists available at ScienceDirect

Journal of Bone Oncology

journal homepage: www.elsevier.com/locate/jbo

Research Paper

Radiomic nomogram for predicting high-risk cytogenetic status in multiple myeloma based on fat-suppressed T2-weighted magnetic resonance imaging

Suwei Liu [a,b,c,d,1], Haojie Pan [b,1], Shenglin Li [a,b,c,d], Zhengxiao Li [a,b,c,d], Jiachen Sun [a,b,c,d], Tiezhu Ren [a,b,c,d], Junlin Zhou [a,b,c,d,*]

[a] Department of Radiology, Lanzhou University Second Hospital, Cuiyingmen No.82, Chengguan District, Lanzhou 730030, China
[b] Second Clinical School, Lanzhou University, Lanzhou, China
[c] Key Laboratory of Medical Imaging of Gansu Province, Lanzhou, China
[d] Gansu International Scientific and Technological Cooperation Base of Medical Imaging Artificial Intelligence, Lanzhou, China

HIGHLIGHTS

- The radiomics signature based on FS-T2WI images could predict HRC Status.
- The radiomics nomogram performed better than the clinical-radiological model, and it might be an easy-to-use supporting tool for HRC status prediction.
- Age, radiomics Rad_score and cytogenetic status play a combined effect on the overall survival of MM patients and are essential factors affecting the prognosis of patients.

ARTICLE INFO

Keywords:
Multiple myeloma
Radiomics
Cytogenetic analysis
Model
Survival analysis

ABSTRACT

Rationale and Objectives: Radiomics has demonstrated potential in predicting the cytogenetic status of multiple myeloma (MM). However, the role of single-sequence radiomic nomograms in predicting the high-risk cytogenetic (HRC) status of MM remains underexplored. This study aims to develop and validate radiomic nomograms based on fat-suppressed T2-weighted images (T2WI-FS) for predicting MM's HRC status, facilitating pre-treatment decision-making and prognostic assessment.

Materials and methods: A cohort of 159 MM patients was included, comprising 71 HRC and 88 non-HRC cases. Regions of interest within the most significant tumor lesions on T2WI-FS images were manually delineated, yielding 1688 features. Fourteen radiomic features were selected using 10-fold cross-validation, employing methods such as variance thresholds, Student's *t*-test, redundancy analysis, and least absolute shrinkage and selection operator (LASSO). Logistic regression was utilized to develop three prediction models: a clinical model (model 1), a T2WI-FS radiomic model (model 2), and a combined clinical-radiomic model (model 3). Receiver operating characteristic (ROC) curves evaluated and compared the diagnostic performance of these models. Kaplan-Meier survival analysis and log-rank tests assessed the prognostic value of the radiomic nomograms.

Results: Models 2 and 3 demonstrated significantly greater diagnostic efficacy compared to model 1 ($p < 0.05$). The areas under the ROC curve for models 1, 2, and 3 were as follows: training set—0.650, 0.832, and 0.846; validation set—0.702, 0.730, and 0.757, respectively. Kaplan-Meier survival analysis indicated comparable prognostic values between the radiomic nomogram and MM cytogenetic status, with log-rank test results ($p < 0.05$) and concordance indices of 0.651 and 0.659, respectively; z-score test results were not statistically significant ($p = 0.153$). Additionally, Kaplan-Meier analysis revealed that patients in the non-HRC group, low-RS group, and aged $\leq$ 60 years exhibited the longest overall survival, while those in the HRC group, high-RS group, and aged $>$ 60 years demonstrated the shortest overall survival ($p = 0.004$, Log-rank test).

* Corresponding author at: Department of Radiology, Lanzhou University Second Hospital, Cuiyingmen No.82, Chengguan District, Lanzhou 730030, China.
E-mail address: ery_zhoujl@lzu.edu.cn (J. Zhou).

[1] Suwei Liu and Haojie Pan contributed equally to the writing of this article.

https://doi.org/10.1016/j.jbo.2024.100617
Received 16 January 2024; Received in revised form 30 May 2024; Accepted 14 June 2024
Available online 15 June 2024

Conclusions: Radiomic nomograms are capable of predicting the HRC status in MM. The cytogenetic status, radiomics model Rad score, and age collectively influence the overall survival of MM patients. These factors potentially contribute to pre-treatment clinical decision-making and prognostic assessment.

1. Introduction

Multiple myeloma (MM), a malignancy marked by the abnormal proliferation of plasma cells, constitutes approximately 1.8 % of all cancers and 18 % of hematologic malignancies in the United States, primarily affecting the bone marrow [1]. The variability in survival times among MM patients, along with their extreme insensitivity to chemotherapy and poor prognosis, may be attributed to unrecognized genetic abnormalities at chromosomal and genetic levels and the absence of effective early-stage treatment modalities [2–3]. The National Comprehensive Cancer Network (NCCN) guidelines and the International Myeloma Working Group (IMWG) diagnostic criteria for risk stratification mandate evaluation of MM patients for cytogenetic markers, including t(4;14), t(14;16), t(14;20), del(17/17p), chromosome 1q amplification, p53 mutations, and non-hyperdiploid karyotypes, identified as high-risk cytogenetic (HRC) factors [4–6]. In HRC patients ineligible for autologous stem cell transplantation, early administration of chemotherapeutic agents such as bortezomib, lenalidomide/carfilzomib, and lenalidomide significantly extends overall survival (OS) [7–8]. Early tandem autologous stem cell transplantation in eligible HRC patients enhances OS [9–10]. Consequently, cytogenetic factors hold significant clinical value in assessing the disease process, selecting treatment options, and predicting prognosis in MM.

Fluorescence in situ hybridization (FISH) of CD138-positive cells is regarded as the gold standard for detecting genetic abnormalities in MM. Additionally, the International Myeloma Working Group (IMWG) consensus recommends evaluating more complex parameters, such as gene expression profiles, mutation detection, and copy number abnormalities [11]. These tests are primarily performed following unilateral bone marrow aspiration or biopsy [2]. However, these invasive procedures increase the risk of clinical infection and economic burden on patients, while yielding samples that do not represent the overall heterogeneity of the disease. Consequently, there is an urgent need to develop non-invasive methods to determine the cytogenetic status of tumors before treatment.

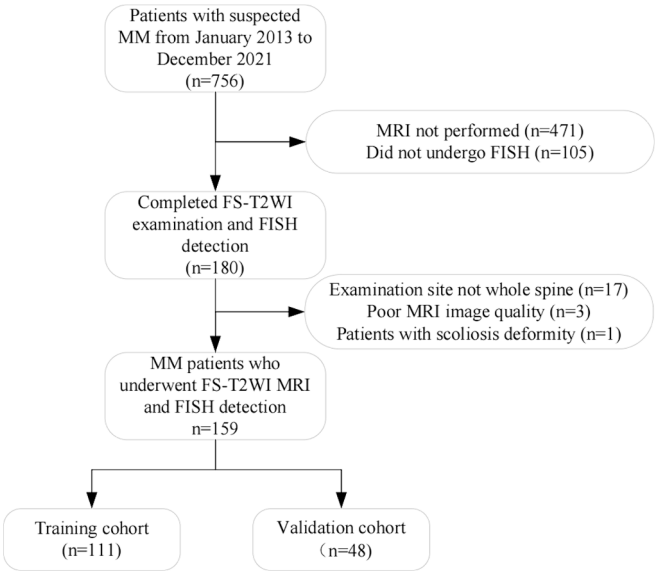

Fig. 1. Flowchart of the patient selection process. MM, multiple myeloma; FISH, fluorescence in situ hybridization; MRI, magnetic resonance imaging; FS-T2WI, fat-suppressed T2-weighted magnetic resonance imaging.

Whole spine magnetic resonance imaging (MRI) is now the preferred diagnostic modality for early detection of bone marrow lesions, owing to its superior soft tissue contrast [12–13]. Fat-suppressed T2-weighted images (T2WI-FS), a standard sequence in whole spine imaging, are critical for diagnosing MM as they enhance the detection of subtle bone marrow edema, allow for comprehensive assessment of bone destruction, and clearly delineate the anatomy of the destruction sites, while eliminating interference from fatty signals [14]. Conversely, conventional MRI findings, such as cumulative vertebral body count and lesion growth patterns, may correlate with cytogenetic status and prognosis [12]. However, these analyses often lack sufficient accuracy and depend heavily on the subjective judgment of radiologists.

Radiomics, a non-invasive imaging-based assessment technique, has recently emerged as a tool for early diagnosis, molecular typing, and prognostic evaluation of diseases by extracting high-throughput imaging data and applying statistical and other analytical methods [15–16]. Previous studies on hematologic radiomics are limited, with recent reports indicating that radiomics facilitates discrimination between HRC and non-HRC statuses in MM [17–18]. However, while these studies developed radiomic models for HRC status using multiple MRI sequences, our study aims to construct and validate a clinical radiomic nomogram based on T2WI-FS sequences, predicting MM cytogenetic status and analyzing its prognostic value in overall survival OS.

2. Materials and methods

The institutional review board at our institution approved this retrospective study and waived the requirement for informed patient consent.

2.1. Patients

This study included 759 patients with pathologically confirmed MM, spanning from January 2013 to December 2021. Inclusion criteria were as follows: 1) pre-treatment T2WI-FS MRI; 2) available FISH results; 3) complete clinical information; 4) presence of at least one vertebral lesion. Exclusion criteria included: 1) non-whole spine examinations; 2) presence of malignant bone metastases or severe scoliosis deformities; 3) poor image quality; 4) non-MM bone marrow or extramedullary lesions. Ultimately, 159 MM cases were included in this study, with a detailed patient selection flow chart provided in Fig. 1. Cytogenetic status was assessed using FISH, with high-risk classification based on the presence of one or more of the following: t(4;14), t(14;16), t(14;20), del(17p), chromosome 1q amplification, p53 mutation, or other chromosomal abnormalities outside of any non-hyperdiploid karyotype. Based on FISH results, patients were categorized into HRC status (71 patients) and non-HRC status (88 patients). Subsequently, the 159 MM cases were randomly allocated into a training cohort (n = 111) and a validation cohort (n = 48) in a 7:3 ratio.

2.2. Follow-up plan

To evaluate the prognostic value of the HRC status prediction model, OS was calculated from the time of initial diagnosis to either the date of death or the study endpoint (December 2021) for patients who remained alive. The median survival time post-diagnosis for each tumor grade determined the minimum follow-up duration for surviving patients, set at 15 months for high-risk and 27 months for non-high-risk groups as per FISH analysis. Patients who did not meet the minimum follow-up

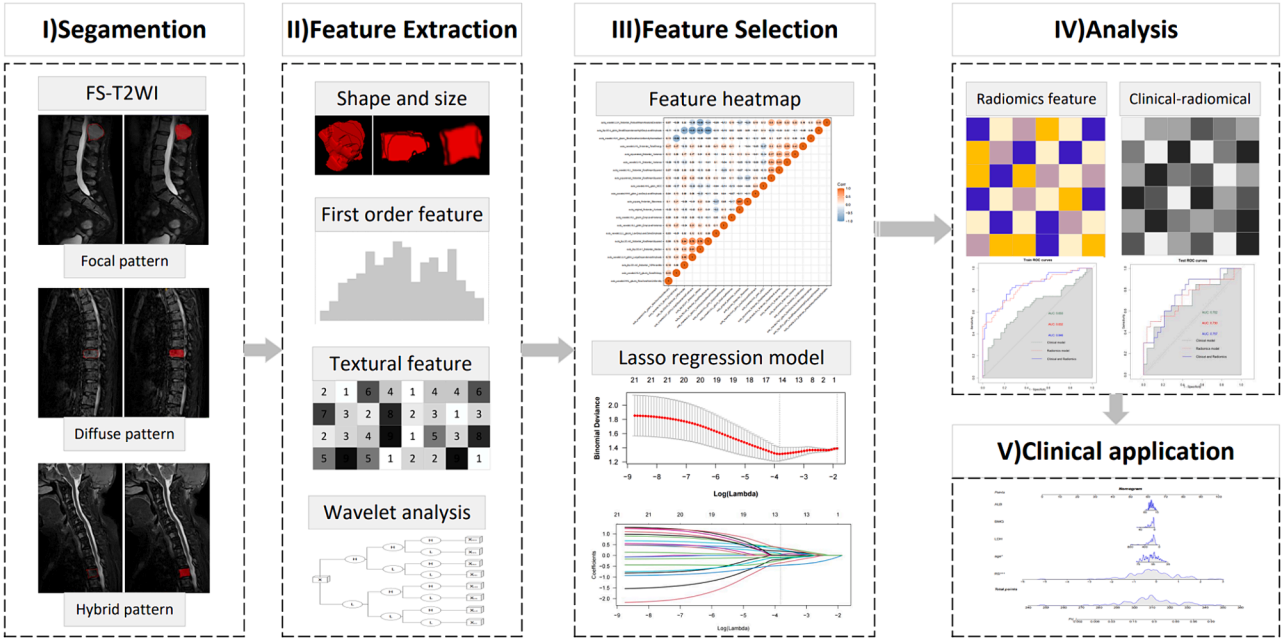

Fig. 2. Flowchart of the MM radiomics approach for predicting cytogenetic status. (I) Manual outlining of the ROI for focal, hybrid, and diffuse lesions. (II) Extraction of image histology features, including shape and size, first-order statistical, texture, and wavelet features. (III) Dimensional reduction of the features using the LASSO regression model. (IV) Combining imaging histological features and clinical features to construct prediction models, further statistical analysis such as ROC curves are used; (V) Finally, column line plots are used to show the MM cytogenetic status prediction results on clinical validity. ROI, region of interest; LASSO, least absolute shrinkage and selection operator; ROC, receiver operating characteristic; MM, multiple myeloma.

Table 1
Characteristics of patients in training and validation cohorts.

Characteristics	Training cohort (N = 111)	*P* value	Validation cohort (N = 48)	*P* value
Cytogenetic Status				
HRC	51(45.95 %)		20 (41.67 %)	
Non-HRC	60 (54.05 %)		28(58.33 %)	
Gender		0.347		0.304
Male	73(65.77 %)		32 (66.67 %)	
Female	38 (34.23 %)		16 (33.33 %)	
Age (Years)	57.42 ± 8.72	0.003*	59.0 ± 10.05	0.049*
BMG	8.93 ± 7.85	0.361	7.029 ± 3.91	0.323
ALB	35.86 ± 7.39	0.645	36.34 ± 8.16	0.806
HB	100.5 ± 27.34	0.323	100.06 ± 29.09	0.118
LDH	219.8 ± 113.95	0.400	198.3 ± 88.34	0.138
MRI Patterns		1.000		0.653
Focal pattern	65 (58.56 %)		29 (60.42 %)	
Diffuse/Hybrid pattren	46 (41.44 %)		19 (39.58 %)	
Compression Fracture		0.097		1.000
Yes	70 (63.06 %)		34 (70.83 %)	
No	41 (36.94 %)		14 (29.17 %)	
Whole Spinal Infiltration		0.421		0.323
Yes	49 (41.14 %)		17 (35.42 %)	
No	62 (58.86 %)		31 (64.58 %)	

Note: *P*-value < 0.05 was considered as a significant difference. "*" represented the Student's *t*-test. "†" represented the Pearson's chi-squared test.
HRC = High-Risk Cytogenetic.
BMG = Beta-2-MicroGlobulin
ALB = Albumin LDH = Lactate Dehydrogenase.

duration or were lost to follow-up were excluded, resulting in 98 of the 159 patients being included in the final analysis. Clinical characteristics of these 98 patients, including age, β2-microglobulin, lactate dehydrogenase, blood albumin, cytogenetic status, OS, MRI lesion growth patterns, and model-stratified risk groups, were collected and analyzed.

Table 2
Results of multivariate logistic regression analysis of three established models in a cohort.

Models	Included variables(*P* value)
Model 1	Age(0.004)
	LDH(0.090)
	BMG(0.323)
	ALB(0.286)
Model 2	auto_lbp.3D.m2_firstorder_10Percentile(0.044)
	auto_lbp.3D.m2_firstorder_RootMeanSquared(0.029)
	auto_original_firstorder_Kurtosis(0.060)
	auto_square_firstorder_Skewness(0.005)
	auto_squareroot_firstorder_RootMeanSquared(0.100)
	auto_squareroot_firstorder_Variance(0.045)
	auto_wavelet.HHH_gldm_LowGrayLevelEmphasis(0.027)
	auto_wavelet.HHL_glszm_SizeZoneNonUniformity(0.016)
	auto_wavelet.HLH_glszm_ZoneEntropy(0.079)
	auto_wavelet.HLL_glrlm_GrayLevelVariance(0.097)
	auto_wavelet.HLL_glszm_GrayLevelVariance(<0.001)
	auto_wavelet.LHL_firstorder_TotalEnergy(0.043)
	auto_wavelet.LLH_gldm_LargeDependenceEmphasis(0.062)
	auto_wavelet.LLL_glszm_LowGrayLevelZoneEmphasis(0.084)
Model 3	Radiomics Score(<0.001)
	Age(0.004)
	LDH(0.090)
	BMG(0.323)
	ALB(0.286)

The p-value for each radiomic feature associated with MM HRC status was calculated using the Mann–Whitney U or Student's t-test.
BMG = Beta-2-MicroGlobulin
ALB = Albumin
LDH = Lactate Dehydrogenase.

Details on MRI data acquisition, region of interest (ROI) segmentation, reproducibility analysis, and radiomic feature extraction are provided in Supplementary S1.

Table 3
Diagnostic performance of three models in the training and validation cohorts.

Cohorts	Models	AUC(95 %CI)	Acc	Sen	Spe	PPV	NPV	Cutoff
Training Set	Model 1	0.650(0.545–0.755)	0.622	0.608	0.683	0.717	0.510	0.469
	Model 2	0.832(0.756–0.908)	0.767	0.706	0.800	0.817	0.686	0.492
	Model 3	0.846(0.771–0.919)	0.748	0.824	0.733	0.817	0.667	0.405
Validation Set	Model 1	0.702(0.547–0.857)	0.667	0.600	0.786	0.786	0.500	0.485
	Model 2	0.730(0.576–0.884)	0.646	0.599	0.929	0.607	0.700	0.784
	Model 3	0.757(0.618–0.896)	0.708	0.900	0.636	0.679	0.750	0.336

AUC = area under the curve;
Acc = Accuracy.
Sen = Sensitivity.
Spe = Specificity.
PPV = positive predictive value;
NPV = positive predictive value;
The cut-off values were determined based on the output value of each predictive model in the training cohort.

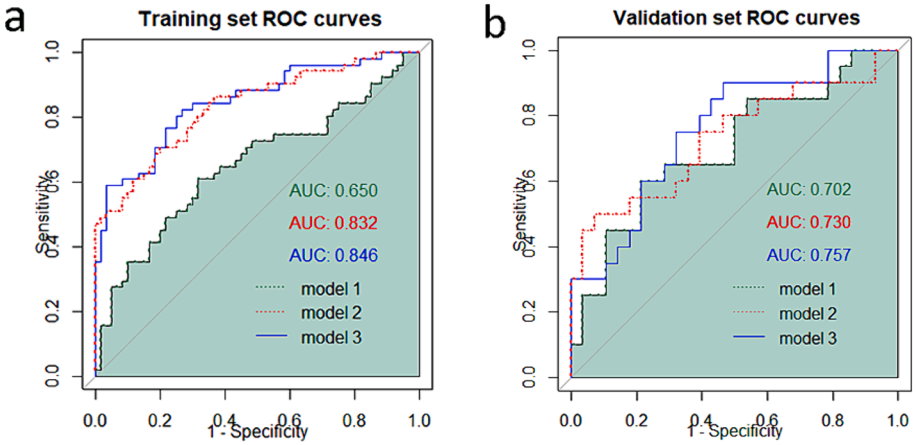

Fig. 3. ROC curves of model 1, model 2, and model 3 are used to predict HRC status in the training (a) and validation sets (b). ROC is the receiver operating characteristic; HRC is the high-risk cytogenetic.

2.3. Radiomic feature selection

Each radiomic feature was initially standardized and normalized, with batch effects—arising from variability in imaging acquisition parameters, scanner models, and reconstruction settings—being removed [19]. Feature screening in the training cohort aimed to eliminate irrelevant and redundant information. Initially, a *variance threshold* was applied to discard features with a variance less than 0.8 [17]. Subsequently, a *batch t-test*, serving as a univariate feature selection method, was used to analyze the relationship between features and classification outcomes using *p*-values. All features yielding *p*-values less than 0.1 were retained. *Redundancy analysis* was then employed to address covariance issues among the features, retaining 21 features with correlation coefficients below 0.8. Finally, the *least absolute shrinkage and selection operator* (LASSO) algorithm was applied to identify the most predictive features within the training cohort. A flow chart detailing this procedure is depicted in Fig. 2.

2.4. Development of the three models.

Model 1: Clinical characteristics by sex and Age and laboratory indices, including blood β2 microglobulin (BMG), blood albumin (ALB), and lactate dehydrogenase (LDH) at the time of initial diagnosis, were studied. A radiologist with 20 years of experience (reader 3) assessed the general imaging features, including mode of lesion growth (focal, mixed, or diffuse), involvement of the entire spinal vertebral body (yes or no), and compression fractures (yes or no). Univariable analysis was used to identify potential clinical-imaging features that differed significantly between the HRC and the non-HRC groups in both the training and validation cohorts. Multifactorial logistic regression analysis was performed on the training cohort to establish model 1.

Model 2: Logistic regression was used to construct a model based on features screened from the FS-T2WI training cohort. 10-fold cross-validation was used to determine the optimal conditioning parameter C to control the trade-off between the training cohort's accuracy and the model's complexity. Model 2 was built using the output of the best radiomic model as the radiomic features.

Model 3: The radiomic features of model 2 were weighted by their coefficients to calculate the radiomic score (RS). The radiomic score from model 2 was combined with model 1 to build model 3. To provide an individualized and easy-to-use tool for predicting the cytogenetic status of patients with MM before treatment, we visualized the combined model as a radiomic nomogram.

2.5. Statistical analysis

Statistical analyses were performed using SPSS software (Version 26.0; IBM et al., N.Y., USA) and R software (https://www.r-project.org; Version 4.1.2). Continuous variables (Age, BMG, ALB, and LDH) between HRC and non-HRC patients were compared using the independent *samples t-test* or the *Mann–Whitney U test*. Categorical variables were compared using the *chi-square test* or the *Fisher test*. Differences were considered statistically significant for $p < 0.05$. The packages in R software involved in this study are shown in Supplementary S2.

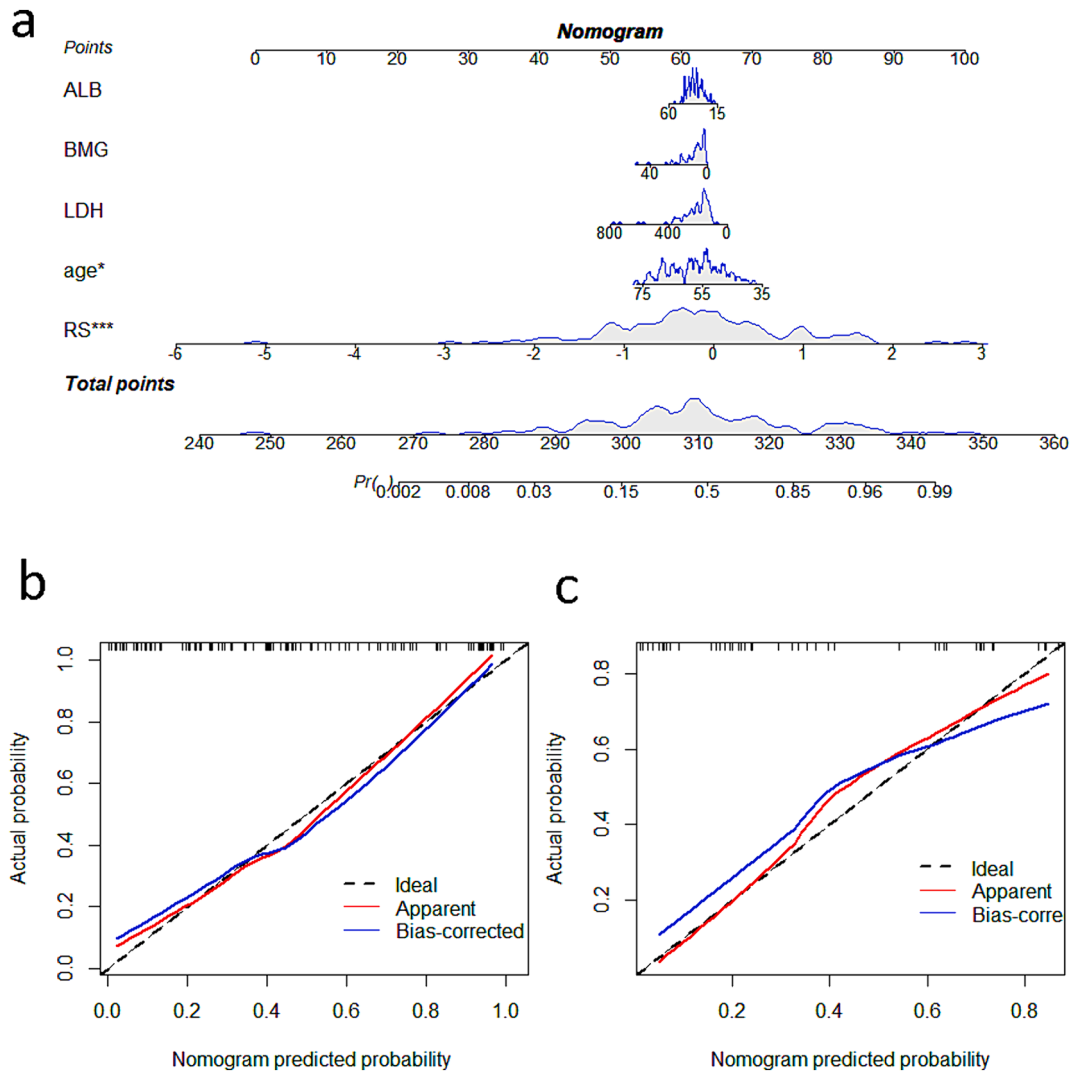

Fig. 4. Clinical practice results. (a) The nomogram shows the use of model 3 in clinical practice. (b,c) Calibration curves of the training and validation sets for the nomogram. The x-axis represents the nomogram-predicted probability, and the y-axis represents the actual probability of MM HRC status. A perfect prediction would correspond to the *45*°dotted black dashed line. The red solid line represents the training cohort(n = 111), and the blue solid line is bias-corrected by bootstrapping (B = 1000 repetitions), indicating observed nomogram performance.

3. Results

3.1. Patient characteristics

The clinical imaging characteristics of MM in the training and validation cohorts are shown in Supplementary S3. We included 88 (55.35 %) patients with HRC status and 71 (46.54 %) with non-HRC status. There was no significant difference in the distribution of cytogenetic status between the training and validation cohorts ($p = 0.619$). There were no significant differences in clinical imaging features between the training and validation cohorts ($p = 0.113$–0.924).

3.2. Feature importance

Of the 1,688 radiomic features, 1,553 had good reproducibility (ICC > 0.9) and were included in the feature selection step. A total of 1,445 features were retained after variance thresholding, 137 features were obtained after the batch *t*-test, 21 were retained after redundancy analysis, and finally, 14 features were retained after LASSO regression and 10-fold cross-validation, including eight wavelet-filtered features and six first-order features.

3.3. Prediction model development, performance, and validation

Model 1: Univariate analysis showed a significant difference in Age (Table 1) between the two groups. A multifactorial logistic analysis determined Age, ALB, BMG, and LDH, combined with clinical significance (Table 2). Model 1 showed diagnostic accuracy of 0.622, AUC of 0.650, sensitivity of 61 %, specificity of 68 %, positive predictive value (PPV) of 72 %, and negative predictive value (NPV) of 51 % (Table 3).

Model 2: The fourteen most predictive features were selected by logistic regression, including eight wavelet-filtered features and six first-order features, as shown in Table 2. Model 2 achieved an accuracy of 0.767, AUC of 0.832, sensitivity of 71 %, specificity of 80 %, PPV of 82 %, and NPV of 69 % (Table 3).

Model 3: The Radiomic Score of the selected features in Model 2 was calculated by weighting them according to their coefficients and including the distribution of the FISH results in the training and validation sets, as shown in Supplementary S4. Multifactorial logistic regression retained Age, ALB, BMG, LDH, and Rad-Score as risk factors (Table 3). Model 3 showed a diagnostic accuracy of 0.748, AUC of 0.846, sensitivity of 82 %, specificity of 73 %, PPV of 82 %, and NPV of 67 % (Table 3).

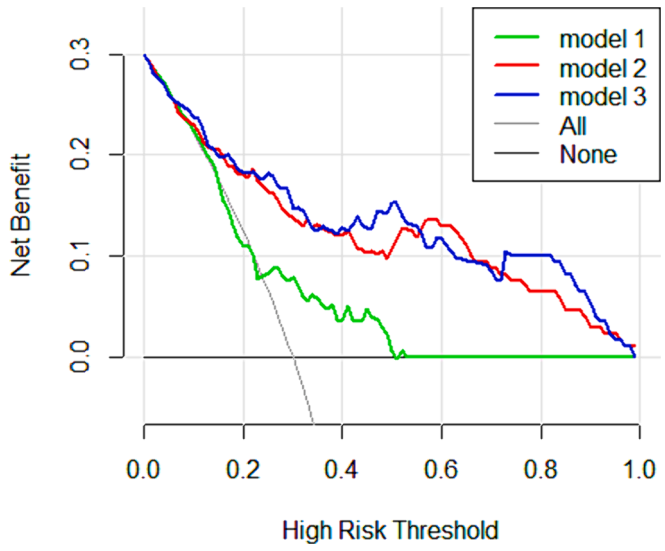

Fig. 5. Decision curve analysis of the three models for predicting MM HRC status. The y-axis measures the net benefits; the green line represents model 1, the red line represents model 2, and the blue line represents model 3. The gray line assumes all patients have a malignant biological behavior prognosis. The black line represents the assumption that no patient has a malignant biological behavior prognosis. The graph demonstrates that if the risk threshold probability is set over 10%, models 2 and 3 have more benefits for predicting MM HRC status than model 1. MM, multiple myeloma; HRC, high-risk cytogenetic.

Table 4
The characteristics of high-risk and low-risk MM in the survival analysis.

Characteristics	High-risk(N = 49)	Low-risk(N = 49)	*P* value
Cytogenetic Status			<0.001***
HRC	33(67.35 %)	8 (16.33 %)	
Non-HRC	16 (32.65 %)	41(83.67 %)	
Age (Years)	56.84 ± 9.13	60.08 ± 9.06	0.048*
BMG	8.67 ± 7.36	8.72 ± 8.34	0.975
ALB	35.44 ± 9.01	36.24 ± 6.93	0.621
LDH	231.1 ± 151.25	213.2 ± 96.22	0.487
MRI Patterns			0.151
Focal pattern	26 (53.06 %)	33 (67.35 %)	
Diffuse/Hybrid pattren	23 (46.94 %)	16 (32.65 %)	
OS (median [range], days)	17.9(2–58)	26.2(1–75)	0.009**

HRC = High-Risk Cytogenetic.
BMG = Beta-2-MicroGlobulin
ALB = Albumin
LDH = Lactate Dehydrogenase.
OS = Overall Survival.
High- and low-RS groups were defined based on scores from a combined model combining age, BMG, ALB, LDH, and radiomic features. For the low-RS group, the score of the integrated model was less than the cutoff; for the high-RS group, that was larger than the cutoff.

3.4. Validation of the models

In the validation cohort, model 1 had a diagnostic accuracy of 0.667, AUC of 0.702, sensitivity of 60 %, specificity of 79 %, PPV of 50 %, and NPV of 49 %. Model 2 had a diagnostic accuracy of 0.646, AUC of 0.730, sensitivity of 60 %, specificity of 93 %, PPV of 61 %, and NPV of 70 %. Model 3 had a diagnostic accuracy of 0.708, AUC of 0.757, sensitivity of 90 %, specificity of 64 %, PPV of 68 %, and NPV of 75 % (Table 3).

3.5. Comparison of the diagnostic performance of the three models

In the training cohort, both model 2 and model 3 had better diagnostic performance and AUC than model 1 ($p < 0.05$, Delong test). In both the training and validation cohorts, the diagnostic performance (AUC) of model 3 was improved over that of model 2, but the difference between the two models was not statistically significant (training: $p = 0.794$; validation: $p = 0.801$), as shown in Fig. 3.

3.6. Clinical usefulness

Model 3 was presented in the form of a nomogram. The calibration curves of the nomogram were confirmed in both the training and validation cohorts (Fig. 4). The Hosmer-Lemeshow test results were insignificant (training: $p = 0.272$; validation: $p = 0.250$). The analysis of decision curves for the three prediction models is given in Fig. 5. The results show that models 2 and 3 have more favorable forecasting ability than model 1 when the risk threshold probability is above 10 %.

3.7. Survival analysis

The clinical characteristics of the 98 patients analyzed are shown in Table 4, where the high- and low-RS groups were defined according to the cutoff value of the joint model (cutoff score = -0.337). Kaplan-Meier analysis showed that MM cytogenetic status and the joint model were associated with statistically significant OS differences between the high- and low-RS groups ($p < 0.05$, log-rank test; Fig. 6). The C-index values for MM cytogenetic status and joint model were 0.651 and 0.659, respectively, and the z-score test showed no significant difference in prognostic values between MM cytogenetic status and joint model ($p = 0.153$).

In addition, integrating the cytogenetic status of MM patients (HRC group vs. non-HRC group), the high- and low-RS and Age (Age > 60 vs. Age ≤ 60) of model 3, all patients were divided into a total of 8 groups (as shown in Fig. 7). The Kaplan-Meier results showed that MM patients in the type = non-HRC group, low-RS group, and Age ≤ 60 had the most extended overall survival, whereas type = HRC group, high-RS group, and MM patients Age > 60 had the shortest overall survival ($p = 0.004$, Log-rank test).

4. Discussion

Our study utilized radiomic nomograms based on T2WI-FS images to predict MM cytogenetic status. The radiomic model, which combines radiomic features with Age, LDH, BMG, and ALB, outperformed the clinical model (AUC 0.846 vs 0.650, $p < 0.05$), demonstrating the incremental value of radiomic features in predicting the cytogenetic status of MM. Furthermore, the combined model stratified MM into high- and low-RS groups based on OS, and its prognostic performance paralleled that of MM cytogenetic status.

Among the clinical risk factors, only Age was an independent predictor of cytogenetic status in MM after univariate and multifactorial analyses, this finding aligns with previous studies that identify Age as the most pertinent factor for cytogenetic status and prognosis, potentially linked to genetic factors that precipitate an earlier age of onset [20–21]. Although previous studies have established a connection between LDH, BMG, ALB, cytogenetic status, and prognosis, BMG levels may reflect tumor load, renal function, and host immune function. In contrast, reduced ALB levels may indicate the impact of interleukin six, produced by the myeloma cell microenvironment, on the liver. Additionally, besides increased capillary permeability and heightened tumor depletion catabolism, inadequate protein intake may also contribute to lower ALB levels in patients with MM [22]. LDH, a glycolytic enzyme in human cells, is widely distributed in leukocytes, erythrocytes, and other organ tissues, typically exhibiting high activity. Serum LDH levels primarily reflect the proliferation, metabolism, and other biological characteristics of LDH-rich cells [23]. Laboratory levels of these malignancies may correlate with cytogenetic status [24–26]. Consequently, we retained LDH, BMG, and ALB as clinically relevant risk factors, enhancing the predictive performance of the clinical model.

Fourteen radiomic features extracted from T2WI-FS MRI images

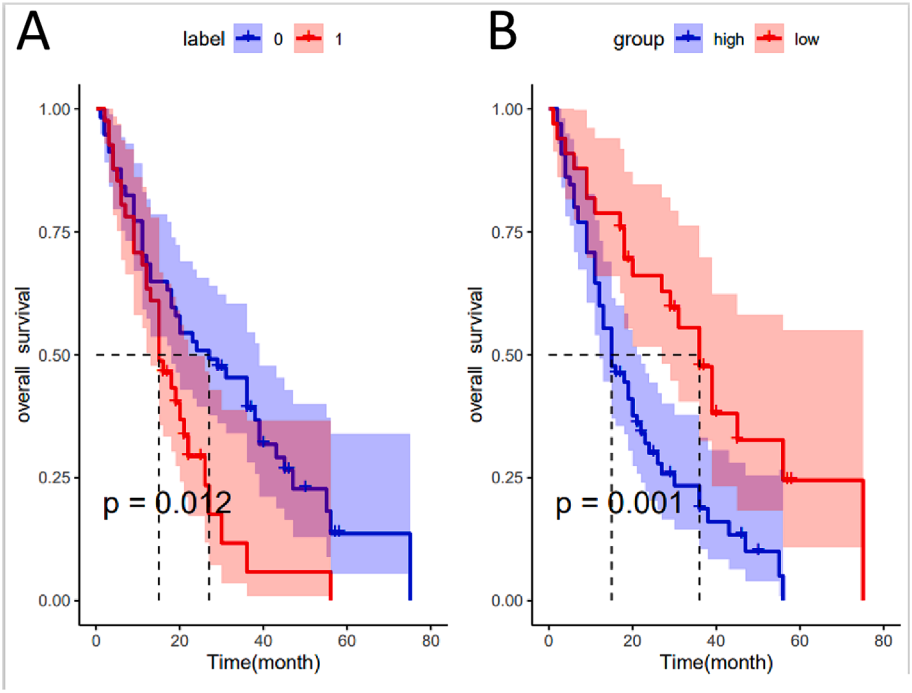

Fig. 6. Kaplan-Meier survival analysis of the cytogenetic status (A) and model 3 (B). The joint model successfully classified MM into high- and low-RS groups with significantly different prognoses, similar to the performance of cytogenetic status.

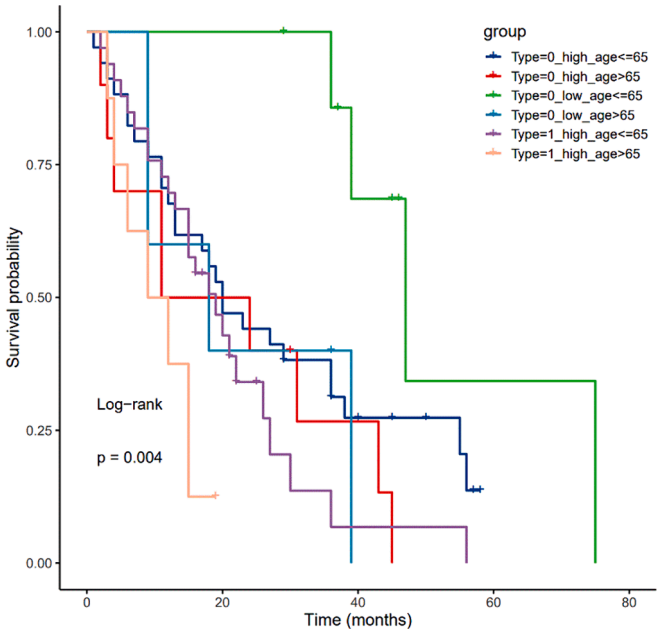

Fig. 7. Kaplan-Meier survival analysis was conducted using the cytogenetic status, Rad_score, and age of MM patients. The results indicated that MM patients in the type = non-HRC group, the low-RS group, and the Age $\leq$ 60 group experienced the longest overall survival, while those in the type = HRC group, the high-RS group, and the Age $>$ 60 group had the shortest overall survival.

showed a high correlation with MM cytogenetic status. Rahmouni et al. [14] suggested that T2WI-FS offers a significant advantage in diagnosing MM spinal lesions, thus, utilizing T2WI-FS single sequence radiomic features can yield crucial information to characterize MM heterogeneity. Furthermore, extracting radiomic features from a single sequence reduces the source data bias linked to the poor alignment of multiple sequences in the spine. Gillies et al. [27] proposed that a binary classifier-based model necessitates ten samples per feature. In our study, we ultimately employed logistic regression to select 14 radiomic features, creating a radiomic model for early prediction of cytogenetic status in MM; similar AUC values were observed between the training and validation cohorts, indicating the absence of overfitting.

Furthermore, the low variability of the results, as demonstrated by the comparative analysis of the ten randomized folds used in cross-validation, suggests stable predictive performance. In this study, 8 of the 14 radiomic features derived from T2WI-FS images in the logistic regression model were wavelet-filtered, and 6 were first-order features, suggesting that both wavelet transform filters and first-order features hold the potential to unveil tumor biology at multiple scales [28]. Wavelet-filtered features can offer more insights into the biological behavior and heterogeneity of tumors than subjective evaluations by radiologists or low-dimensional radiomics, as demonstrated in studies on intrahepatic cholangiocarcinoma, renal cell carcinoma, prostate cancer, and bladder cancer [29–32]. Conversely, first-order features provide more reproducible low-dimensional information, as evidenced in cystic renal masses and coronary atherosclerotic disease [33–34]. Consequently, our results indicate that the radiomic features of T2WI-FS MRI images can independently delineate differences in the cytogenetic status of patients with MM.

The model that combines radiomic features and clinical factors outperformed the clinical model, demonstrating the incremental value of radiomic features in predicting MM cytogenetics. Finally, we employed nomograms to visualize pre-treatment decisions for MM cytogenetic status, the outcomes of which are yet to be determined. Combined modeling of nomograms could serve as an effective and user-friendly adjunct tool to estimate MM cytogenetic status pre-treatment via non-invasive diagnostic methods, particularly for patients unable to undergo biopsy or cytogenetic examination.

Moreover, the present study evaluated the prognostic value of the combined model, an excellent contribution to current radiomics studies of cytogenetic status in MM patients, enabling direct demonstration of clinical relevance. In this study, MM patients with non-HRC status derived greater benefit from treatment and exhibited longer OS compared with those with HRC status, consistent with previous studies

that identified cytogenetic status as a crucial prognostic marker for MM patients. Additionally, this study categorized MM samples into high-RS and low-RS groups based on the Rad_score from the combined model. We demonstrated that the radiomics model Rad_score offers prognostic value comparable to that of cytogenetic status. We found that cytogenetic status, the radiomics model Rad_score, and age collectively influence the overall survival of MM patients. These factors can predict patient prognosis to a certain extent.

5. Limitations

It should be noted that our study has some limitations. We did not subdivide MM into multiple immunoglobulin types, a direction that may be explored in subsequent studies. Conversely, our analysis was limited to T2WI-FS images; future studies should integrate more sequences and clinical parameters for enhanced comparative analysis modeling. Accordingly, our results demonstrate that even single-sequence T2WI-FS images can achieve promising predictive power compared to other studies. Moreover, while we explored the model's impact on the prognostic assessment of MM patients and concluded that the Rad_score can serve as a critical factor in assessing prognosis, constructing a predictive model for MM prognosis remains an unmet challenge, which will be addressed in our future work.

6. Conclusion

In summary, a radiomic nomogram based on T2WI-FS sequences can predict MM cytogenetic status more accurately than a purely clinical model, enabling risk stratification of MM according to OS. Additionally, age, the radiomics Rad_score, and cytogenetic status collectively impact the overall survival of MM patients. These factors are crucial in affecting patient prognosis, assisting in pre-treatment decision-making that includes chemotherapy regimens and planning for autologous stem cell transplantation, and are particularly beneficial for future targeted therapy decisions.

7. Authorship

All those designated as authors could meet all four criteria for authorship.

CRediT authorship contribution statement

Suwei Liu: Writing – review & editing, Writing – original draft, Visualization, Validation, Supervision, Software, Resources, Project administration, Methodology, Investigation, Funding acquisition, Formal analysis, Data curation, Conceptualization. **Haojie Pan:** Writing – original draft, Validation, Software, Resources, Investigation, Formal analysis, Data curation. **Shenglin Li:** Supervision, Software, Resources, Project administration, Investigation, Funding acquisition. **Zhengxiao Li:** Funding acquisition, Formal analysis, Data curation. **Jiachen Sun:** Supervision, Software, Resources, Project administration, Methodology. **Tiezhu Ren:** Visualization, Validation, Supervision, Project administration, Methodology. **Junlin Zhou:** Writing – review & editing, Visualization, Validation, Supervision, Software, Resources, Project administration, Investigation, Formal analysis, Data curation, Conceptualization.

Declaration of competing interest

The authors declare that they have no known competing financial interests or personal relationships that could have appeared to influence the work reported in this paper.

Acknowledgment

Suwei Liu, Haojie Pan, Shenglin Li, Zhengxiao Li, Jiachen Sun, Tiezhu Ren, Junlin Zhou.

Ethical approval

Ethical approval (2023A-168) was obtained from our institutional ethics review board; the requirement for informed consent was waived owing to the study's retrospective nature.

Appendix A. Supplementary data

Supplementary data to this article can be found online at https://doi.org/10.1016/j.jbo.2024.100617.

References

[1] R.L. Siegel, K.D. Miller, A. Jemal, Cancer statistics, 2020, CA Cancer J. Clin. 70 (1) (2020) 7–30.
[2] S.K. Kumar, V. Rajkumar, R.A. Kyle, et al., Multiple Myeloma, Nat. Rev. Dis. Primers 3 (2017) 17046.
[3] C.Y. Soekojo, T.H. Chung, M.S. Furqan, W.J. Chng, Genomic characterization of functional high-risk multiple myeloma patients, Blood Cancer J. 12 (1) (2022) 24.
[4] S.K. Kumar, N.S. Callander, J. Hillengass, et al., NCCN Guidelines Insights: Multiple Myeloma, Version 1.2020, J. Natl. Compr. Canc. Netw. 17 (10) (2019) 1154–1165.
[5] S.K. Kumar, N.S. Callander, K. Adekola, et al., Multiple Myeloma, Version 3.2021, NCCN Clinical Practice Guidelines in Oncology, J. Natl. Compr. Canc. Netw. 18 (12) (2020) 1685–1717.
[6] N.S. Callander, M. Baljevic, K. Adekola, et al., NCCN Guidelines® Insights: Multiple Myeloma, Version 3.2022, J. Natl. Compr. Canc. Netw. 20 (1) (2022) 8–19.
[7] M.V. Mateos, M. Cavo, J. Blade, et al., Overall survival with daratumumab, bortezomib, melphalan, and prednisone in newly diagnosed multiple myeloma (ALCYONE): a randomised, open-label, phase 3 trial, Lancet 395 (10218) (2020) 132–141.
[8] T. Facon, C.P. Venner, N.J. Bahlis, et al., Oral ixazomib, lenalidomide, and dexamethasone for transplant-ineligible patients with newly diagnosed multiple myeloma, Blood 137 (26) (2021) 3616–3628.
[9] J. Blocka, T. Hielscher, H. Goldschmidt, J. Hillengass, Response Improvement Rather than Response Status after First Autologous Stem Cell Transplantation Is a Significant Prognostic Factor for Survival Benefit from Tandem Compared with Single Transplantation in Multiple Myeloma Patients, Biol. Blood Marrow Transplant. 26 (7) (2020) 1280–1287.
[10] M. Cavo, F.M. Gay, F. Patriarca, et al., Double Autologous Stem Cell Transplantation Significantly Prolongs Progression-Free Survival and Overall Survival in Comparison with Single Autotransplantation in Newly Diagnosed Multiple Myeloma: An Analysis of Phase 3 EMN02/HO95 Study, Blood 130 (2017) 401.
[11] E.M. Ocio, P.G. Richardson, S.V. Rajkumar, et al., New drugs and novel mechanisms of action in multiple myeloma in 2013: a report from the International Myeloma Working Group (IMWG), Leukemia 28 (3) (2014) 525–542.
[12] J. Hillengass, K. Fechtner, M.A. Weber, et al., Prognostic significance of focal lesions in whole-body magnetic resonance imaging in patients with asymptomatic multiple myeloma, J. Clin. Oncol. 28 (9) (2010) 1606–1610.
[13] E. Zamagni, P. Tacchetti, M. Cavo, Imaging in multiple myeloma: How? When? Blood 133 (7) (2019) 644–651.
[14] A. Rahmouni, M. Divine, D. Mathieu, et al., Detection of multiple myeloma involving the spine: efficacy of fat-suppression and contrast-enhanced MR imaging, AJR Am. J. Roentgenol. 160 (5) (1993) 1049–1052.
[15] M. Hatt, C.C. Le Rest, F. Tixier, B. Badic, U. Schick, D. Visvikis, Radiomics: Data Are Also Images, J. Nucl. Med. 60 (Suppl 2) (2019) 38s–44s.
[16] Z. Liu, S. Wang, D. Dong, et al., The Applications of Radiomics in Precision Diagnosis and Treatment of Oncology: Opportunities and Challenges, Theranostics 9 (5) (2019) 1303–1322.
[17] J. Liu, C. Wang, W. Guo, et al., A preliminary study using spinal MRI-based radiomics to predict high-risk cytogenetic abnormalities in multiple myeloma, Radiol. Med. 126 (9) (2021) 1226–1235.
[18] J. Liu, P. Zeng, W. Guo, et al., Prediction of High-Risk Cytogenetic Status in Multiple Myeloma Based on Magnetic Resonance Imaging: Utility of Radiomics and Comparison of Machine Learning Methods, J. Magn. Reson. Imaging 54 (4) (2021) 1303–1311.
[19] I. Shiri, M. Amini, M. Nazari, et al., Impact of feature harmonization on radiogenomics analysis: Prediction of EGFR and KRAS mutations from non-small cell lung cancer PET/CT images, Comput. Biol. Med. 142 (2022) 105230.
[20] S.Z. Usmani, P. Rodriguez-Otero, M. Bhutani, M.V. Mateos, J.S. Miguel, Defining and treating high-risk multiple myeloma, Leukemia 29 (11) (2015) 2119–2125.
[21] M. Zamani-Ahmadmahmudi, S.M. Nassiri, F. Soltaninezhad, Development of an RNA sequencing-based prognostic gene signature in multiple myeloma, Br. J. Haematol. 192 (2) (2021) 310–321.
[22] P.R. Greipp, J. San Miguel, B.G. Durie, et al., International staging system for multiple myeloma, J. Clin. Oncol. 23 (15) (2005) 3412–3420.

[23] A. Palumbo, H. Avet-Loiseau, S. Oliva, et al., Revised International Staging System for Multiple Myeloma: A Report From International Myeloma Working Group, J. Clin. Oncol. 33 (26) (2015) 2863–2869.
[24] N.H. Abdallah, M. Binder, S.V. Rajkumar, et al., A simple additive staging system for newly diagnosed multiple myeloma, Blood Cancer J. 12 (1) (2022) 21.
[25] J. Shaughnessy Jr., E. Tian, J. Sawyer, et al., Prognostic impact of cytogenetic and interphase fluorescence in situ hybridization-defined chromosome 13 deletion in multiple myeloma: early results of total therapy II, Br. J. Haematol. 120 (1) (2003) 44–52.
[26] S. Oh, D.H. Koo, M.J. Kwon, et al., Chromosome 13 deletion and hypodiploidy on conventional cytogenetics are robust prognostic factors in Korean multiple myeloma patients: web-based multicenter registry study, Ann. Hematol. 93 (8) (2014) 1353–1361.
[27] R.J. Gillies, P.E. Kinahan, H. Hricak, Radiomics: Images Are More than Pictures, They Are Data, Radiology 278 (2) (2016) 563–577.
[28] J.J.M. van Griethuysen, A. Fedorov, C. Parmar, et al., Computational Radiomics System to Decode the Radiographic Phenotype, Cancer Res. 77 (21) (2017) e104–e107.
[29] Y. Zhou, G. Zhou, J. Zhang, C. Xu, X. Wang, P. Xu, Radiomics signature on dynamic contrast-enhanced MR images: a potential imaging biomarker for prediction of microvascular invasion in mass-forming intrahepatic cholangiocarcinoma, Eur. Radiol. 31 (9) (2021) 6846–6855.
[30] T.Y. Kim, N.H. Cho, G.B. Jeong, E. Bengtsson, H.K. Choi, 3D texture analysis in renal cell carcinoma tissue image grading, Comput. Math. Methods Med. 2014 (2014) 536217.
[31] S. Bhattacharjee, C.H. Kim, H.G. Park, et al., Multi-Features Classification of Prostate Carcinoma Observed in Histological Sections: Analysis of Wavelet-Based Texture and Colour Features, Cancers (basel) 11 (12) (2019).
[32] Z. Zheng, Z. Gu, F. Xu, et al., Magnetic resonance imaging-based radiomics signature for preoperative prediction of Ki67 expression in bladder cancer, Cancer Imaging 21 (1) (2021) 65.
[33] A. Könik, N. Miskin, Y. Guo, A.B. Shinagare, L. Qin, Robustness and performance of radiomic features in diagnosing cystic renal masses, Abdom Radiol (NY) 46 (11) (2021) 5260–5267.
[34] M. Kolossváry, J. Karády, Y. Kikuchi, et al., Radiomics versus Visual and Histogram-based Assessment to Identify Atheromatous Lesions at Coronary CT Angiography: An ex Vivo Study, Radiology 293 (1) (2019) 89–96.